5
Multifunctional OFETs with HfO_2/Gelatin Gate Dielectric

OFETs have opened up new possibilities as key elements for smart intelligent systems, due to capability of processing multiple functionalities in a single device. The ongoing development of multifunctional OFETs advances the field of flexible and wearable electronics by integrating traditional transistor functions with additional sensing, memory, circuitry, and actuation capabilities. Such emerging devices are generally fabricated using functionalized organic semiconductors and gate dielectrics which respond to external stimuli such as light, temperature, humidity, or chemical analytes, making them suitable for applications in health monitoring, environmental sensing, and smart packaging. Generally, hybrid integration of multiple devices is required to perform multiple applications in a system, which eventually enhances the need of a wide range of materials, cost, and complexity of the processes. However, devices like OFETs can exhibit these qualities by suitable optimization and selection of component materials and also can significantly suppress the fabrication complexity. The use of natural materials with additional sensing functionalities have shown promise in biosensing with providing the possibility of biodegradability and biocompatibility in devices. Furthermore, these high-performance devices can be used to implement circuitry, making them suitable candidates for real applications. In this chapter, a hybrid bilayer gate dielectric combination of natural polymer and inorganic oxide dielectric is employed with a photosensitive active layer to demonstrate high-performance OFETs with excellent sensing capabilities towards humidity, UV, and visible light, along with circuit capability. The findings presented in this chapter have been recently published (Konwar, Saxena, Raghuwanshi, et al., 2022b).

5.1 INTRODUCTION

OFET is an essential building block of flexible electronics that has gained tremendous popularity due to its inherent advantages and compatibility with rigid as well as flexible substrates like cloth, paper, plastic skin, etc (Sirringhaus, 2014; Wu et al., 2018). Demonstration of multifunctional OFETs are becoming an important aspect, which can perform diverse functionalities along with tradition transistor characteristics. To perform multifunctionality in a system, integration of various devices is needed which requires a wide range of materials, enhancing the cost of the systems and complicating the procedures. Utilizing the functionalities of organic semiconductors, gate dielectrics, OFETs have the potential to perform multifunctioanl apllications for different applications like sensing, memory, and circuitry (Wu et al., 2015; Zarei et al., 2023). In multifunctional OFETs, various external stimuli can regulate the charge transportation along with traditional charge transport behavior due to the applied gate electric field, providing diverse functionalities beyond basic electronic switching capabilities (C. A. Di et al., 2013). Multifunctional OFET devices can simplify the overall fabrication complexity and reduce the system costs significantly (Q. Liu et al., 2020; Park et al., 2021; B. Yang et al., 2020). Recently, various OFET-based sensors, light-emitting transistors, photodetectors, and memory cells, highlighting the rapid development of multifunctional OFETs are demonstrated (Chaudhry et al., 2020; C. Wang et al., 2020), though this area is still underexplored. The use of natural polymer components for exploring functionalities is rare, which is important for biodegradable and eco-friendly electronics with integrating additional functionalities.

Moreover, the performance of OFETs is determined by various factors starting from the properties of the substrate to organic semiconductor material, dielectric, device structure, and semiconductor dielectric interface (Sachin Rahi et al., 2022; Wu et al., 2018). A high quality dielectric: semiconductor interface is preferred to reduce the charge trapping, which is influenced by various factors such as structural defects in the semiconductor film or grain boundaries, surface roughness, polar functional group, and dielectric constant (k) of gate dielectric (Ortiz et al., 2010; Sachin Rahi et al., 2022). Gelatin is one of the most widely used natural proteins, exhibiting high performances at low operating voltage (Mandal et al., 2020a; Mao, Hwang, et al., 2014), however, a pristine layer of this protein-based dielectric faces gate leakage current issues (Mandal et al., 2020a; Mao, Hwang, et al., 2014), they have been used in a demonstration of high performance OFETs. Integrating a thin high-k metal oxide dielectrics along with these polymer layers helps in achieving highly oriented semiconductor layers on top of the dielectric and supports mitigating both leakage and high operating voltage concerns in OFETs (Ortiz et al., 2010; Yang et al., 2008). HfO_2 is the most widely used dielectric (Gao et al., 2017; He et al., 2013; G. He et al., 2014; Gang He et al., 2014; Zhang et al., 2014) in bilayer combinations due to its high dielectric constant (k~20-25), and low temperature (~100 °C) processing capabilities for high quality, dense, and pinholes free films of precise thickness control up to a few nanometers with help of techniques such as Atomic Layer Deposition (ALD). Recently, various biopolymers and nature-inspired materials have emerged as vital components in the fabrication of eco-friendly devices (Baek et al., 2018; Di Mauro et al., 2021; Pradhan et al., 2020). The use of natural polymer components for exploring functionalities is rare. Table 5.1 summarizes the performance of some recently reported p-channel OFETs with pristine natural proteins or with a bilayer of high-k dielectrics along with their additional functionalities if any. Most of these reports with natural dielectrics demonstrate transistors with thermally evaporated OSCs such as pentacene as an active layer and reports with solution-processed OSCs with these dielectric combinations are scarce (Ranjodh Singh et al., 2017).

In this paper, flexible OFET devices are demonstrated with HfO_2/gelatin gate dielectric and TIPS-Pentacene as an active layer. TIPS-Pentacene was used as a photosensitive layer, which shows good light sensitivity toward visible and UV range (D. Bharti et al., 2017; Feng et al., 2024). Neat TIPS-Pentacene layer is preferred for light-sensing applications due to the presence of higher interfacial trapped densities for the trapping of photogenerated electrons during illumination (Mahato et al., 2019). Moreover, neat TIPS-Pentacene devices exhibited maximum change in carrier concentration towards the blue lights discussed earlier by our group (D. Bharti et al., 2017). These fabricated flexible OFET devices exhibit excellent electrical characteristics with high field-effect mobility reaching over 2 cm^2/Vs (extracted with C_i at 1 kHz), low subthreshold swing (SS) of ~0.20 V/dec., and high I_{on}/I_{off} ratio at a low operating voltage of -5 V with excellent electrical and mechanical stability. Moreover, circuit and multi-parameter sensing capabilities such as for visible and UV light, as well as the humidity and breath rate have been successfully demonstrated from these devices. The inverter applications are demonstrated with various ranges of external load resistance. Our results indicate that these multifunctional OFET devices can open up a plethora of opportunities for practical applications such as real-time health and environment monitoring.

Table 5.1 : Summary of some recently reported p-channel OFETs with a natural protein or and high-k/ natural protein hybrid bilayer gate dielectrics.

Dielectric	OSC	OSC Process	Op.V (V)	V_{TH} (V)	μ_{avg} (cm^2/Vs)	Functionality	Ref.
Collagen	Pentacene	Evaporated	- 45	- 12	0.8	Transistor	(Hsieh et al., 2013)
Bovine serum albumen	Pentacene	Evaporated	- 40	- 16	0.30	Transistor	(Lee et al., 2013)

Keratin	P3HT	Sol. Processed	- 7	- 1	2.2×10^{-3}	Transistor	(Ranjodh Singh et al., 2017)
Silk fibroin	Pentacene	Evaporated	- 80	- 40	0.35	Transistor	(Baek et al., 2018)
Gelatin	TIPS-PEN	Sol. Processed	- 5	-0.5	3.4	Inverter, humidity sensing	(Raghuwanshi et al., 2020)
AlO_x/ Adenine	Pentacene	Evaporated	-12.5	-	0.35	Transistor	(Mihai Irimia-Vladu et al., 2010)
Al_2O_3/ Cellulose	Pentacene	Evaporated	- 3	-0.9	0.10	Inverter	(Petritz et al., 2013)
Al_2O_3/ Gelatin	Pentacene	Evaporated	- 2	-1.05	0.33	Humidity sensing	(Mandal et al., 2020a)
Gum arabic	DPPTTT/PMMA	Sol. Processed	-3	-0.35	0.6	Transistor	(Seck, Mohammadian, Diallo, Faraji, Saadi, et al., 2020)
HfO_2/ Gelatin	TIPS-PEN	Sol. Processed	- 5	- 0.9	2.1	Inverter, light and humidity sensing	This work

5.2 Device Fabrication and Electrical Characterization

OFETs with BGTC device structure were fabricated on a flexible ITO-coated PET substrate, with ITO acting as gate electrodes. Substrates of sizes 3 cm × 4 cm were cleaned with a conventional cleaning process and pasted on a rigid glass substrate for support. A 40 nm thick HfO_2 was deposited through ALD at 100 °C by using tetrakis(dimethylamido)hafnium (TDMAH) and H_2O precursors. Further, gelatin solution was prepared by dissolving in DI with similar process as explanind in section Chapter 4. A 0.5 wt. % TIPS-Pentacene solution in toluene was prepared by mixing it for 2.5 hours at 65 °C and drop cast over the dielectric. A solvent-rich closed environment was provided for slow drying to achieve a uniform crystalline film of semiconductors. Finally, Au top source/drain electrodes were deposited through shadow masks. The schematic and digital images of fabricated devices are shown in Figure 5.1 (a) and (b) respectively with bottom gate top contact configuration.

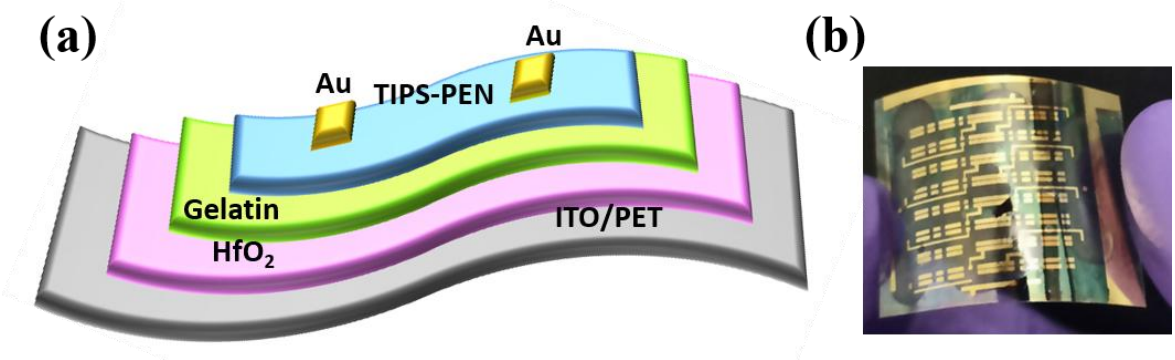


Figure 5.1 : (a) Schematic of bottom gate top contact OFET devices with high-k HfO2/gelatin bilayer gate dielectric, (b) digital image of fabricated devices.

All the fabrications processes and electrical characterizations were carried out in ambient conditions. Electrical characteristics were measured using Keithley 4200 SCS analyzer. To calculate the C_i, a metal-insulator-metal (MIM) structure of ITO-HfO_2/gelatin- Au was designed and measured value at 1 kHz and found to be 8.2 (± 0.6) nF/cm^2. The dielectric constant of gelating was extracted to be ~5. In this approach, a reduced value of capacitance density is obtained due to the series coupling of bilayer gate dielectrics. All the device parameters were calculated from the transfer characteristics. Effects of visible and UV light along with humidity and breath rate were also analyzed by exposing these to devices. The fluctuation of device parameters was optimized from these.

5.3 RESULTS AND DISCUSSION

5.3.1 Investigation of Surface Morphology and Film Crystallinity

Surface morphology of bilayer dielectrics and TIPS-Pentacene films was observed through atomic force microscopy (AFM) images obtained from SPM XE-70 AFM system and shown in Figure 5.2 (a) and (b) respectively. A very smooth surface morphology with a roughness of 0.48 (±0.10) nm was obtained for HfO_2/gelatin bilayer gate dielectric film, which is essential for ordered semiconductor growth with lesser trapping sites and low gate leakage current. The structured growth of TIPS-Pentacene crystal over dielectric was achieved as shown in Figure 5.2 (b), which was also obtained in previous studies. The crystallinity behavior of TIPS-Pentacene film was explained by XRD measurements exhibiting a high degree of crystallinity oriented more in (001) plane direction. FWHM is calculated for a highly oriented plan and found to be ~1.3. Less value of FWHM indicates higher crystallinity, which is beneficial for device performance.

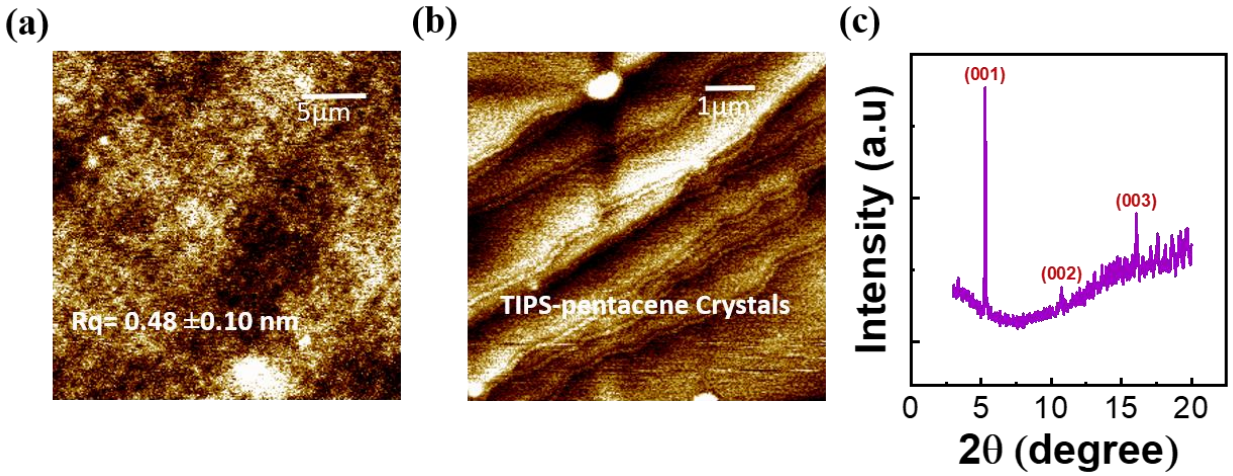


Figure 5.2 : Surface morphology of (a) HfO2/Gelatin bilayer, and (b) TIPS-Pentacene crystal. (c) XRD pattern for TIPS-Pentacene.

5.3.2 Electrical Characteristics and Transistor Performance

The electrical property of the dielectric layer was characterized by measuring the current density through the MIM structure of ITO-HfO_2/gelatin-Au, and shown in Figure 5.3 (a). The primary objective of using 40 nm thick HfO_2 layer was to suppress the gate leakage, along with overall enhancement in the dielectric properties. A significantly low leakage current density was obtained from a hybrid bilayer dielectric which is highly desirable for low-voltage operating devices. Transfer and output characteristics of a representative fabricated device are shown in Figure 5. 3 (b) and (c) respectively. As can be seen from these characteristics, these devices have shown excellent p-channel characteristics at a voltage of -5 V. Usually, the capacitance density for gelatin must be calculated at a lower frequency due to the requirement for longer polarization time. Here, it was calculated at 1 kHz, which is the lowest possible frequency for our available module Keithley 4200 SCS analyzer. The devices exhibited maximum field-effect mobility up to ~2.1 cm^2/Vs and V_{TH} of - 0.9 (± 0.3) V with I_{on}/I_{off} of ~10^4. The extracted mobility values will certainly be lower if C_i for low frequency is used, as per earlier reports (Mandal et al., 2020a). Moreover, in multiple instances in literature, C_i values obtained from the range 1kHz to 1MHz

were used to extract the mobility values from devices with gelatin as a dielectric component, though mostly for vacuum evaporated semiconductors (C.-J. Lee et al., 2019; Mao, Gan, et al., 2014; Mao, Hwang, et al., 2014). In addition, k_p which is a normalized performance parameter, can be used for a fair comparison with other reports in this case.

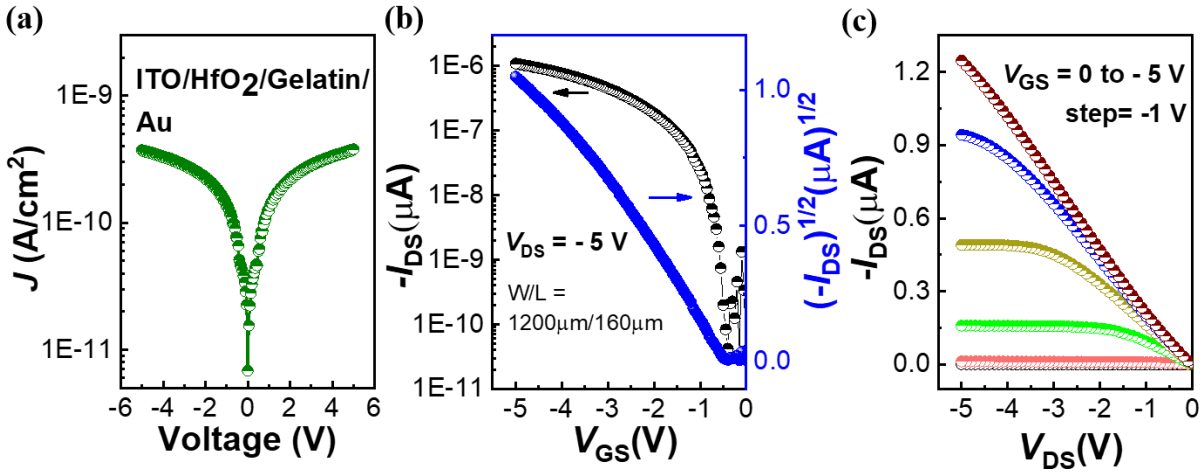


Figure 5.3: (a) *J-V* characteristics of ITO- HfO_2/gelatin-Au (b) Transfer and (c) output characteristics for a particular OFET device.

An average and maximum value of 9.0 and 17.2 nF/Vs for k_p, were achieved in these devices, very similar to 9.1 and 19.9 nF/Vs for high-performance OFET devices with TIPS-Pentacene (Raghuwanshi, Bharti, & Tiwari, 2016). *SS* and interfacial trap density (D_{it}) were calculated to be 200 mV/decade and 1.3×10^{11} $cm^{-2}eV^{-1}$ respectively. These *SS* and D_{it} values must be lower for faster switching of devices. This high performance is achieved due to the combined effect of bilayer gate dielectric properties. The average transit frequency of the devices was estimated to be ~550 Hz as per method suggested earlier (Klauk, 2018). These values are certainly low but suitable for many real time sensing and health monitoring applications where desired frequency of operations is very low (D. I. Kim et al., 2015). Moreover, as *L* of the devices are large (100 to 250 μm) and the source drain electrodes are completely overlapping with gate, these devices were expected to offer lower transit frequencies. Patterned gate electrodes can help in enhancing the speed of operation. The water molecules present in the gelatin film allow high performance in ambient conditions. The residues of acidic and basic amino acids reacted with the absorbed water molecules and generates mobile protons. In the presence of an external field, the mobile protons moves towards electrodes, forming EDLs at the dielectric: semiconductor and dielectric: gate electrode interfaces, providing comparatively high capacitance density (Mao, Hwang, et al., 2014). This protein film dielectric is found to be suitable for the fabrication of high-performance flexible OFETs in ambient conditions. Here, the second dielectric layer HfO_2 is used to minimize the leakage current and operating voltage.

Table 5.2 : Summary of obtained electrical parameters with HfO_2/gelatin gate dielectric

C_i (nF/cm^2)	$k_{p,max}$ (nF/Vs)	$\mu_{sat\ (avg)}$ (cm^2/Vs)	μ_{max} (cm^2/Vs)	V_{TH} (V)	I_{on}/I_{off}	SS (V/dec)	D_{it} ($cm^{-2}\ eV^{-1}$)
8.2 ± 0.6	17.2	1.1 ± 0.8	2.1	- 0.9 ± 0.3	~ 10^4	0.20	1.3×10^{11}

5.3.3 Repeatability, Bias-stress, and Environment Stability

The operational stability of devices were investigated through the continuous scanning of transfer curves for 100 times and bias-stress stability for utilizing in practical applications. These results of multiple continuous scans of transfer characteristics are shown in Figure 5.4 (a) and (b). As can be seen from these results, good repeatability was observed upon multiple continuous

scans. The change in I_{DS} and V_{TH} over the scans are shown in Figure 5.4 (b). For bias-stress, a constant voltage of V_{DS} = V_{GS} = -5 V was applied for 1 hour with 30 s pulse duration. The I_{DS} was recorded after each pulse and observed its variation during the period. Decay of normalized I_{DS} and variations of V_{TH} during the stress period are shown in Figure 5.4 (c). The current is decaying with time due to the trapping of charge carriers at the semiconductor: dielectric interface. This trapping can happen due to the presence of polar groups in the gelatin biopolymer. However, the polar dielectric can enhance the I_{DS} during the polarization time by causing excess charge carriers at the dielectric/semiconductor interface and decrease during the stress period by trapping them. This type of trapping is common in polar dielectrics. Further, environmental stability for these devices in normal ambient conditions was studied up to 12 weeks. A comparison of transfer characteristics for pristine and after 12 weeks of exposure in normal ambient for a particular device is shown in Figure 5.4 (d). As it can be seen, extremely low variation in the characteristics was observed indicating excellent shelf-life stability.

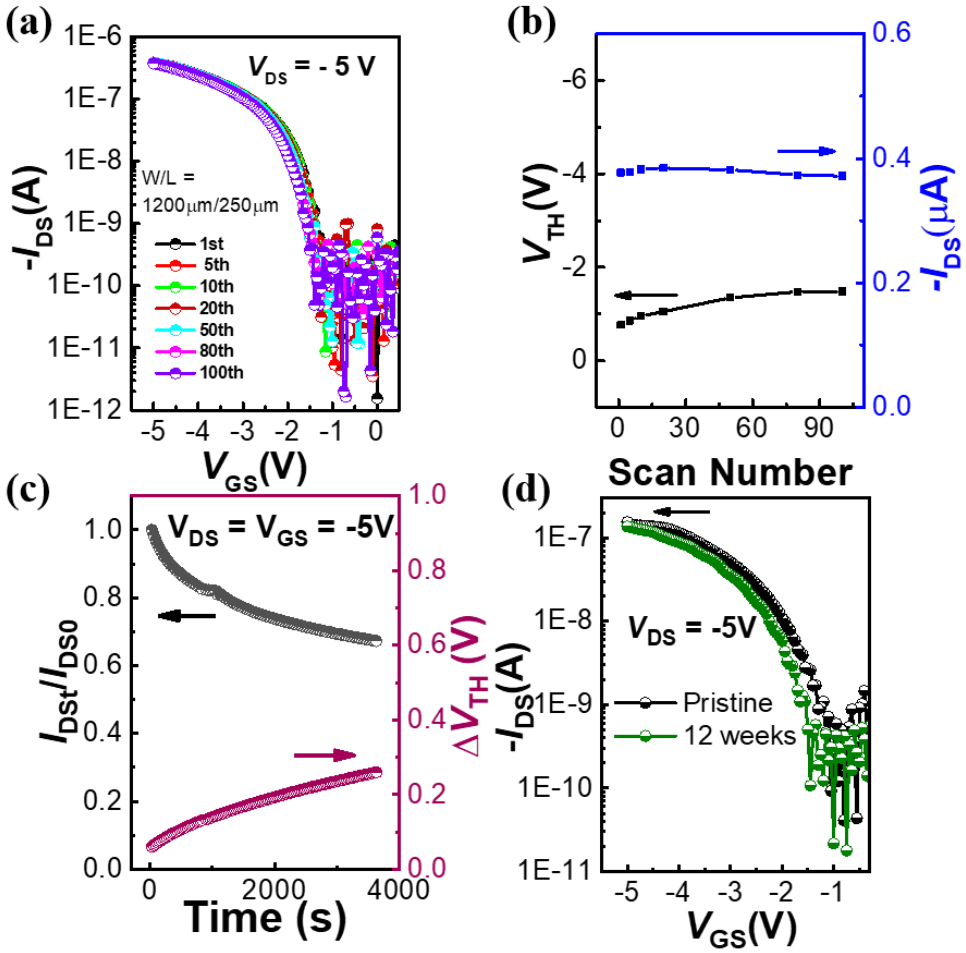


Figure 5.4: (a) Multiple scanning of transfer characteristics, (b) change in V_{TH} and I_{DS} over scan period, (c) normalized I_{DS} and Δ V_{TH} for a bias-stress test, and (d) shelf-life or environmental stability for 12 weeks.

5.3.4 Resistive Load Inverter

The circuit application for these devices was explored using a resistive load inverter. Resistive load inverter circuits were implemented with external load resistors R_L (10 MΩ - 50 MΩ) connected with these p-channel OFETs to study the switching behavior of the devices in circuits for -5V operation (V_{DD} = -5V). The corresponding voltage transfer curves for each R_L value with input voltage (V_{in}) sweep from 0 to -5 V are shown in Figure 5. 5 (a). When V_{in} is lower than V_{TH}, the OFET is in OFF condition with almost nil output current (I_{DS}) leading to V_{out} almost equal to V_{DD}. Hence, at low input, a perfect high state or logic 1 state occurs for all values of R_L. At high V_{in} relatively low state or logic 0 state is obtained as expected from these circuits. For resistive load inverters, the output voltage (V_{out}) is given by the following equation.

$$V_{out} = V_{DD} - I_{DS}.R_L \quad (5.2)$$

As per this equation, for small R_L, the output swing will be lower with high value of the output when input reaches V_{DD}. As it can be seen for R_L of 10 MΩ. Voltage transfer characteristics were improved on increasing the R_L value as the voltage drop across this high resistance becomes higher. Hence, with high R_L, significantly better voltage transfer characteristics were obtained. The same is confirmed as per the results obtained for R_L of 50 MΩ. Further to analyze the switching characteristics of inverter circuit, a time-dependent dynamic response was demonstrated with a load resistance of 50 MΩ by giving a square wave pulse input between 0 and -5 V at the gate terminal shown in Figure 5. 5 (b). A good dynamic response between (-5 and -1) was obtained indicating high switching of the inverter.

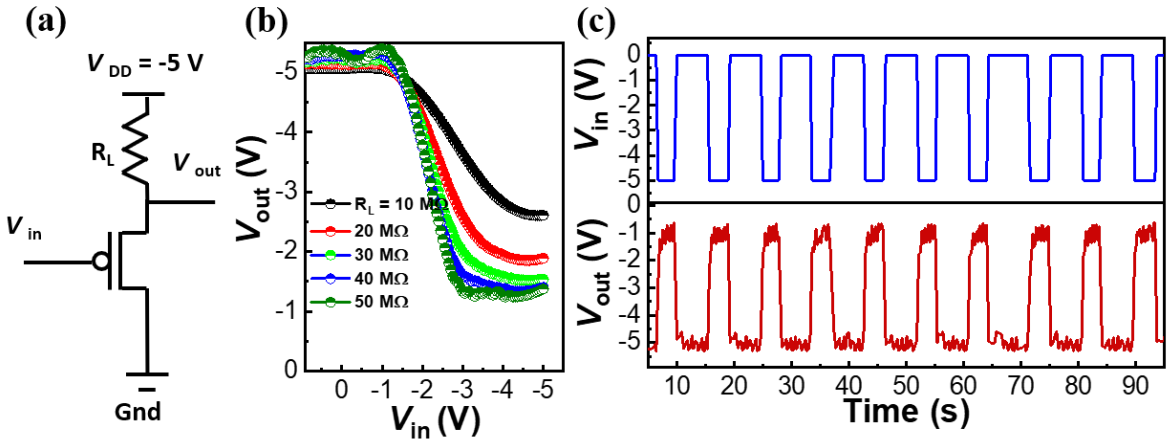


Figure 5.5 : (a) Resistive load inverter circuit, (a) voltage-transfer curve with varying load resistance from 10 to 50 MΩ, and (c) dynamic behavior for 50 MΩ resistance.

5.3.5 Humidity Sensing

Gelatin has a high water-absorbing property that will improve the overall performance of the device in a humid environment. As a result of this distinguishing feature, it is suitable to use as a humidity sensor in various industry applications, including health monitoring, food processing, etc. In this study, the characteristics of devices were investigated by exposing them to a humid environment as shown in Figure 5.6 (a). In this study, humidity pulses refer to exhaled human breath from mouth ranging from 42% to 90% RH, as measured by commercial humidity sensor placed near the devices.

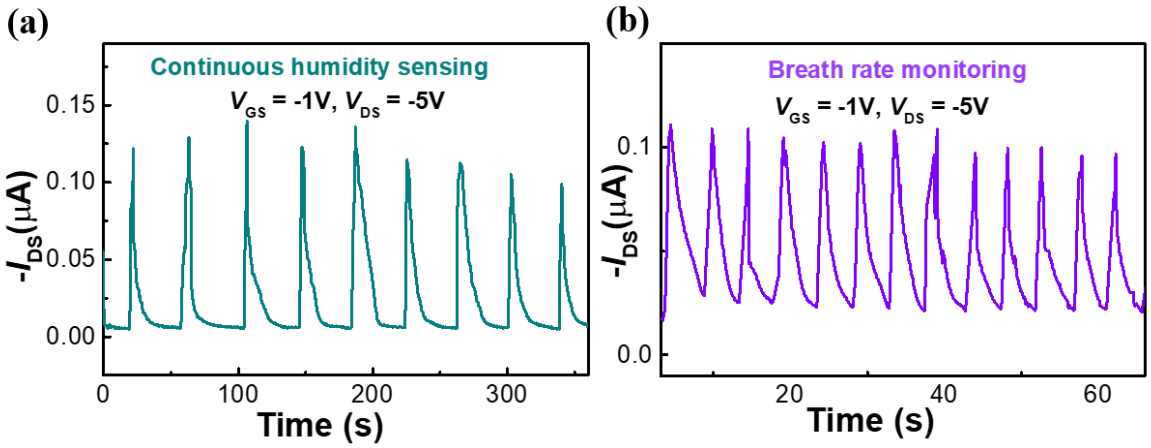


Figure 5.6 : Change in drain current on exposing continuous humidity (a), and breath rate (b), for V_{GS} = -1 V and V_{DS} = -5 V.

The device was kept at V_{GS} = -1 V and V_{DS} = -5 V and continuously subjected to humidity pulses, and observed that the I_{DS} abruptly rose on exposure to the humidity and gradually decreased to the initial base value once it was removed. This phenomenon happens due to the production of extra charges on absorbing water molecules, which enhances the charge accumulation at the dielectric: semiconductor interface which eventually raises the device current. Due to the hygroscopic nature of gelatin, water molecules interact with the polar -OH groups in ammonic acid in gelatin film and form negatively charged ions, hence it changes the electrical properties of OFETs (Mandal et al., 2020a; Mao, Hwang, et al., 2014). The number of absorbed water molecules is directly proportional to the relative humidity level. In a humid environment, adsorbed water molecules reacted with the functional groups and dissociated into mobile ions. In presence of water molecules, carboxyl groups dissociate into carboxylate ions ($-COO^-$) and protons and the amine groups are protonated to form ammonium (NH_3^+) ions. Additionally, water adsorption forms hydrogen-bonded networks in the material, which creates a conducting pathway between neighbouring water molecules or functional groups to hop protons produced by hydronium ions via the Grotthuss mechanism. High proton concentration leads to higher ionic conductivity, enabling the formation of strong EDL at the dielectric: semiconductor interface. Thus, capacitance density across the MIM (ITO/HfO_2/gelatin/Au) structure has increased at higher humidity levels, due to higher electrical permittivity of water than gelatin and contribute to high carrier conductions and increases the I_{DS} with respect to humidity level (Shapardanis et al., 2014). From the result, it is observed that gelatin device reaches saturation very quickly just after exposure to humidity, similarly during desorption process it reaches to initial stage with less time, which makes it suitable for highly sensitive humidity sensors. To investigate their practical utility, continuous breath rate is monitored by changing the humidity exposure while exhaling and inhaling the breathing. The quick change in drain current is obtained with the change in humidity and is shown in Figure 5. 6 (b). During the experiment, the devices were positioned in close proximity to the nose and exposed to exhaled breath at regular intervals to simulate sudden changes in ambient humidity. Here, in this experiment 12 breaths/minute can be detected without any failure confirming the suitability of devices as highly sensitive real-time breath sensors for health monitoring.

5.3.6 Light Sensing

The impact of light on fabricated devices was observed by illuminating various ranges of visible (red, $\lambda \sim 620$ nm; green, $\lambda \sim 520$ nm; and blue, $\lambda \sim 460$ nm) and UV light ($\lambda = 365$ nm). Here, TIPS-Pentacene acts as a photosensitive active layer and responds to the various luminous intensities at different wavelengths. Out of all three ranges of visible lights, blue has a greater influence on TIPS-Pentacene due to its higher luminous intensity than the other two bands (D. Bharti et al., 2017). Moreover, the absorption coefficient of blue light is less, and due to this excitons can be generated in the bulk or near the dielectric semiconductor interface, contributing to the photoconductive phenomenon. Figure 5.7 (a) and (c) depict the transfer characteristics taken in the dark environment and after turning ON the blue light and UV light respectively throughout the observation. Generally, two different mechanisms: photoconduction and photovoltaic have been observed in OFET under light irradiations. The photovoltaic mode is observed in the accumulation region, when the device is in a turn-on state. Most of the reported outcomes are related to the photoconduction effect which is observed in a turn-off state or the device operates in a depletion region. The conductivity of the organic layer increases in direct correlation with the optical power intensity due to enhanced carrier mobility or density (J. Liu et al., 2020). Photons are adsorbed at the TIPS-Pentacene surface on illumaniting light and leads to the generation of excitons, which are then dissociated to free electron-hole pairs after application of an electric field. The photo-generated electrons are partly trapped at the interface of semiconductor: dielectric under external biasing conditions, lowering the available trapped densities which eventually reduced the device's V_{TH} (Mahato, Bharti, Saxena, et al., 2021; Mahato, Bharti, Varun, et al., 2021).

However, the photo-generated holes drift readily towards the drain terminal, improving the device's I_{DS}. The output response of these devices is the summation of field-generated carriers and

photo-induced carriers. The photo effect is more significant near and below the V_{TH} as the photo carriers are abundant in this regime. However, at the higher V_{GS}, the photoresponse gets suppressed due to the presence of surplus field-induced carriers. Figure 5.7 (b) and (d) demonstrate the time-resolved photoresponse characteristics under continuously incident periodic light pulses. The I_{DS} is observed at V_{GS} = -1 V and V_{DS} = -5 V in the interval of 0.05 s. Whenever the light is turned ON, the I_{DS} increases quickly due to rapid collections of photo-generated holes at the drain terminal; however, later the response slows down while the photo-generated free charge carriers are being trapped at the -OH riched gelatin surface. Under dark conditions, while the illumination is turned OFF, I_{DS} decays slowly due to poor recombinations of charge carriers and finally reaches the initial value. Maximum values of photoresponsivity (R) for blue and UV light were found to be 10 mA/Watt and 14 mA/Watt respectively as calculated using a standard formula (D. Bharti et al., 2017). Moreover, the current modulation (P) of ~8 and ~22 were observed respectively for blue and UV light, which was extracted from the transfer characteristics. Though these values are on the lower side, this aspect adds an additional functionality in the devices.

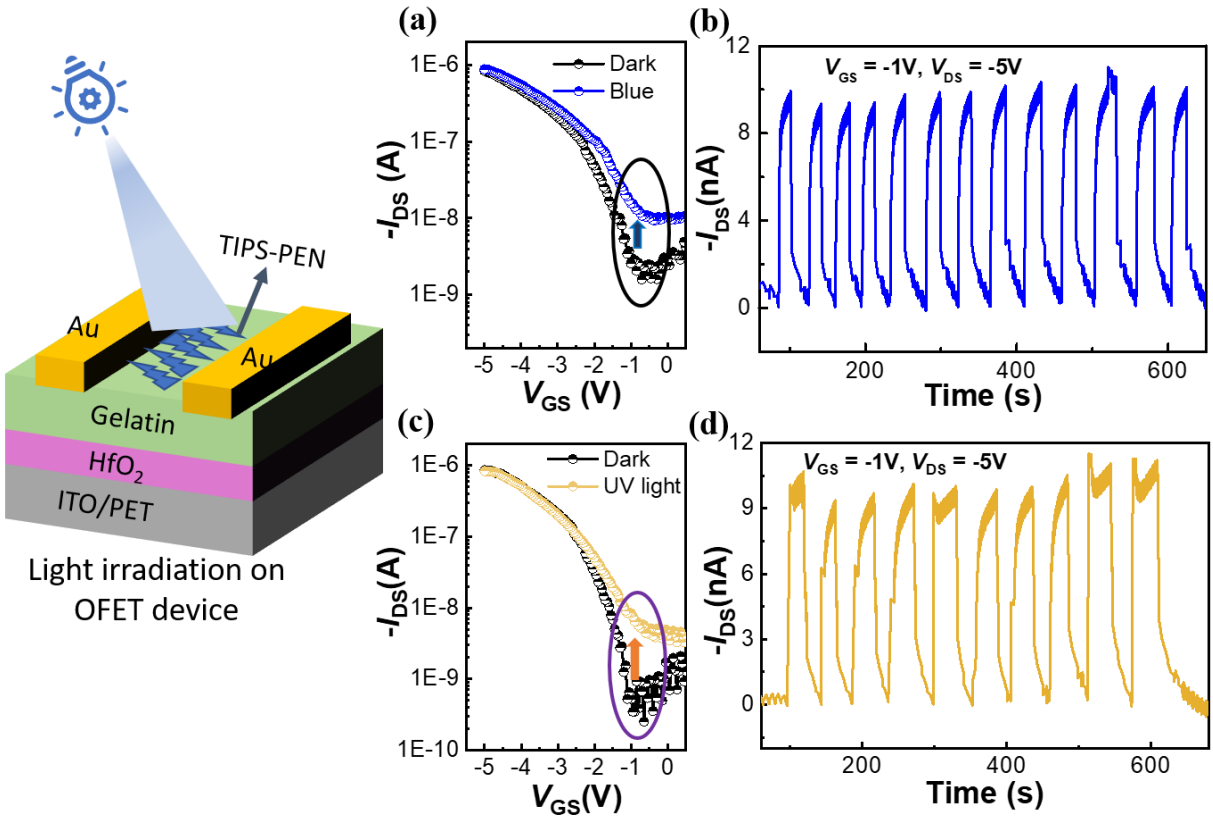


Figure 5.7 : Effects of visible and UV lights on device's output response. Change in transfer behavior after illumination of blue (a) and UV light (c). Time-dependent I_{DS} on continuously applying pulses of blue (b), and UV light (d).

5.3.7 Effect of Bending on Transistor Performance

Besides the multifunctional properties, sustaining the functional properties and reliability after mechanical deformation or bending is crucial for the integration of these devices for flexible systems. Figure 5.8 summarizes the effect of bending on transfer characteristics. To study the same, a strain was applied on devices with a fixed bending radius of 12.5 mm for 15 minutes and changes in electrical performances due to the effect of this bending were studied. Figure 5.8 (a) shows the bending strategy for a fabricated sample by mounting it on a curved surface to maintain a fixed bending radius. Figure 5.8 (b) shows the transfer characteristics before and after bending for a particular OFET device under test. A small variation in current was observed with good p-channel behavior even after bending the devices. A minimum shift of V_{TH} with reduced I_{DS} was

observed due to the trapping of charges at the semiconductor bulk and dielectric: semiconductor interfaces. All the electrical parameters were calculated and found to be an average μ of 0.8(± 0.5) cm^2/Vs and a maximum μ of ~ 1.6 $cm^2/$ Vs. The remaining parameters V_{TH}, SS, and D_{it} are - 1(± 0.1) V, 370 mV/decade, and 2.7 $\times 10^{11}$ cm^{-2} eV^{-1} respectively. From the results, it can be estimated that the device performances do not degrade much after applying the deformation, indicating decent electromechanical stability for future flexible and printed electronics. This reduced performance can be influenced by several factors starting from the formation and proliferation of microcracks or defects in the semiconducting film due to the breakage of semiconductor crystals during strain, or it could be caused by variations in the gelatin film's characteristics. Repeatability of devices was optimized again scanning the transfer characteristics up to 100 cycles. Overlapping transfer behavior on one over another is observed with minimal variation of output current. Figure 5.8 (c) and (d) demonstrate the multiple scanning characteristics and their variations of V_{TH} and I_{DS}.

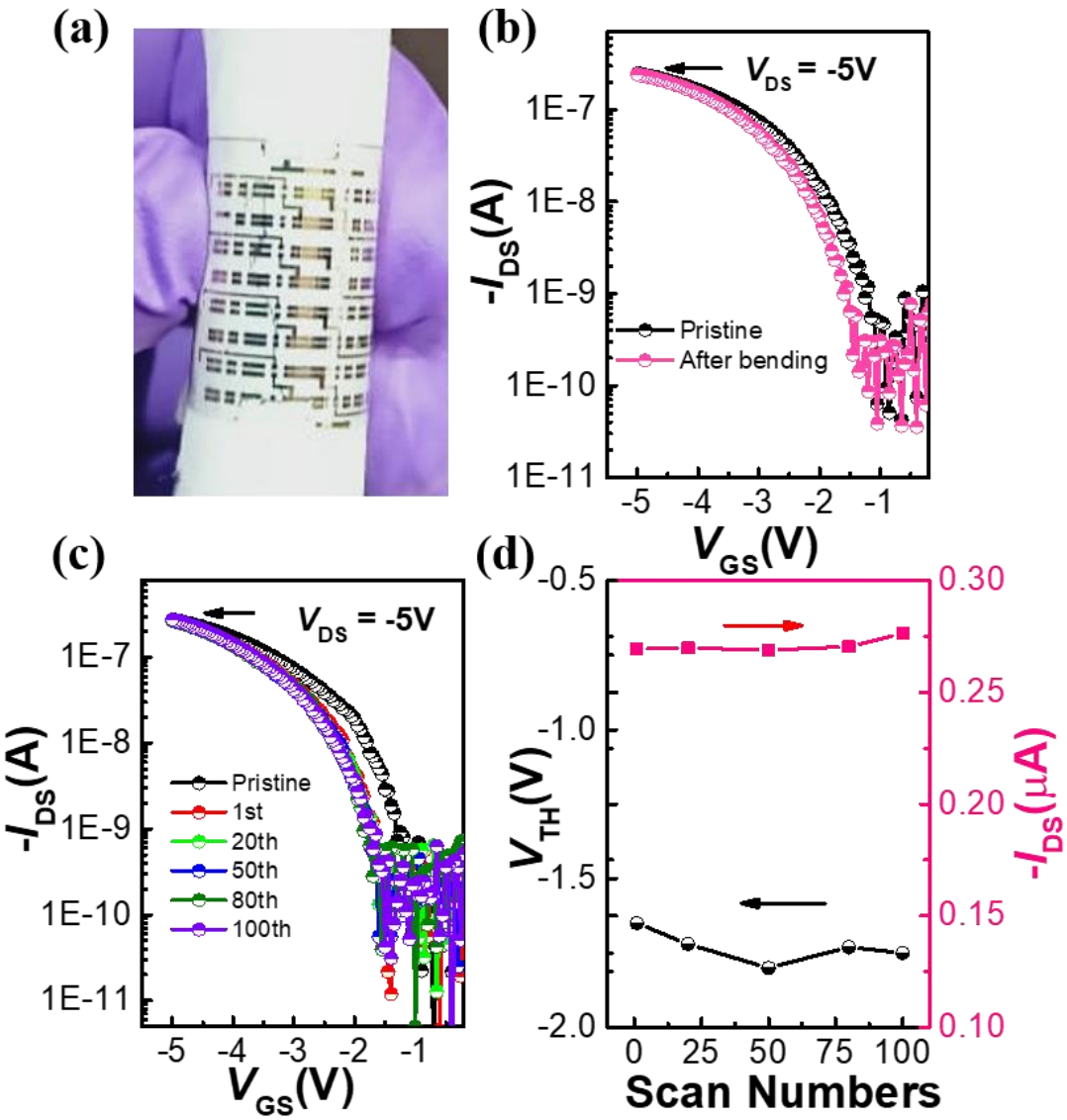


Figure 5.8 : (a) Bending strategy for a fabricated sample by mounting on a curved surface, (b) typical transfer characteristics before and after bending, (c) repeatability test, and (d) variation of V_{TH} and I_{DS} for 100 cycles.

In addition, both the sensing mechanisms for light and humidity were obtained and shown in Figure 5.9. The effect of blue and UV light on device performance is almost similar to the before bending characteristics and is demonstrated in the plots Figure 5.9 (a) and (b). The dynamic response of I_{DS} for continuous light pulses is also investigated for both the lights and shown in the given plots. A quick response is noticed on I_{DS}, providing the feasibility of these sensors in flexible substrates. Also, the humidity sensor characteristics were investigated by changing

humidity around the devices, and continuously monitoring breath rate for two minutes, which are shown in Figure 5.9 (c) and (d). A very high response with higher stability is observed, indicating that this device could be easily mounted on human body or flexible substrates for continuous health monitoring purposes. The integration of all these applications in this proposed device configuration leads to a new path toward the fabrication of multifunctional OFETs as well as the incorporation of biodegradable materials in sensors for implantable electronics.

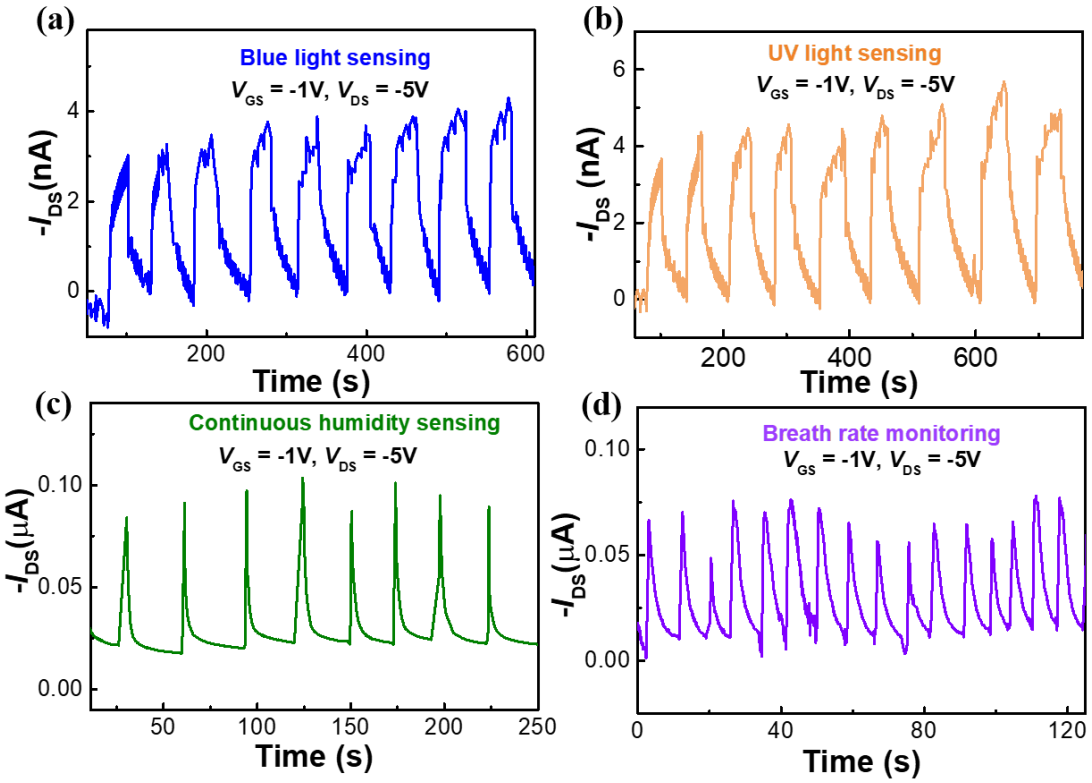


Figure 5.9 : Sensing for blue light (a), UV light (b), humidity (c), and breath rate (d), after application of tensile bending.

5.4 CONCLUSION

In this chapter, multifunctional flexible OFETs were demonstrated using a bilayer gate dilectric of HfO_2/gelatin and TIPS-Pentacene as an active layer. The reported bilayer inorganic/organic combination helps to suppress the leakage current density and exhibits excellent electrical characteristics with μ_{max} of ~ 2.1 cm^2/Vs (for C_i at 1 kHz) in saturation regime at -5 V in OFET devices. Excellent electrical stability was observed from multiple scanning of transfer behavior up to 100 cycles. In addition, the inverter characteristics were analyzed to determine the possibility of these devices in circuit applications. The effects of light intensity and humidity were studied to investigate the multifunctional behavior of these OFET devices. Due to the high sensitivity of gelatin towards humidity, this bilayer combination shows excellent performance as a humidity sensor demonstrates real-time breath monitoring. In contrast the Chapter 4, the present chapter primarily emphasizes the multifunctional capabilities of these devices rather than focusing solely on achieving high transistor performance. Three crucial applications integrated into a single OFET device make it an attractive choice for the exploration of smart e-textile applications.

…